NANO · MICRO small
www.small-journal.com

Synthesis of Hydrogen-Substituted Graphyne Film for Lithium–Sulfur Battery Applications

Jiaqiang Li, Sha Li, Qing Liu, Chen Yin, Lianming Tong, Changguo Chen, and Jin Zhang**

Graphyne (GY) is a new type of carbon allotrope, which is viewed as a rapidly rising star in the carbon family referred to as 2D carbon allotropes due to its extraordinary properties. Considering the dynamic nature of the alkyne metathesis reaction, a hydrogen-substituted graphyne (HsGY) film is successfully synthesized on a gas/liquid interface using 1,3,5-tripynylbenzene (TPB) as the precursor. The synthesized HsGY film is used as a sulfur host matrix to be applied in lithium–sulfur batteries (LSBs). The HsGY@S electrode is prepared using S_8 as sulfur source and presents excellent electrochemical performance.

Carbon, one of the most fascinating elements in the periodic table, has three kinds of hybridization states, namely, sp, sp^2, and sp^3 hybridized carbon atoms, which could make up different carbon nanomaterials.[1] Since the Nobel Prize winning discovery of fullerene, many efforts have been devoted to synthesize new kind of carbon allotropes, such as carbon nanotube and graphene, which are constructed by sp^2 hydride carbon atoms.[2–4] As a consequence of abundant outstanding properties of these diverse carbon allotropes, they have been applied to advance applications in the fields of water purification,[5] catalyst support,[6,7] sensing,[8] and energy storage and conversion.[5,9–11]

Graphyne (GY) is a new branch of carbon allotropes, which consists of sp and sp^2 hybrid carbon atoms.[12,13] In 1987, Begaman first proposed several forms of GY based on the different combining forms of sp and sp^2 hybrid carbon atoms.[14] The γ-GY, generally called GY, can be formally viewed as a result from the replacement of one-third of the carbon–carbon bonds in graphite by acetylic linkages (—C≡C—).[14,15] Since the first propose of GY, many studies focused on the investigation of their theoretical properties based on different calculation methods.[16–18] However, the approaches for GY synthesis are being developed slowly. Graphdiyne (GDY) is an important member in GY family that contains diacetylene linkages (—C≡C—C≡C—) connecting adjacent benzene rings extending in 2D plane.[19] GDY can be synthesized through alkyne coupling reaction using hexaethynylbenzene (HEB) as precursor.[20–23] However, the synthesis of GY structure is an ongoing challenge and the most difficult thing is how to construct the acetylic linkages. Usually, there are two synthetic routes: Pd/Cu-catalyzed coupling reactions and alkyne metathesis reactions. The former usually obtain ethynylene-linked polymers and often suffer from dehalogenation side reactions and contamination with Pd catalysts residues.[24,25] Alkyne metathesis is a kind of dynamic covalent reactions that are wildly used for various organic compounds and materials synthesis.[26] The dynamic nature of alkyne metathesis leads to self-correction mechanisms and allows the molecular structure formed under thermodynamic control, enhancing the formation of highly ordered structures rather than amorphous materials.[24,27,28] Therefore, alkyne metathesis reaction is a candidate reaction for GY synthesis. The serious challenge is how to rationally design and synthesize precursors, catalysts, and ligands, and then synthesize GY with desirable topology and thickness. Obviously, the hexapropynylbenzene (HPB) is the most suitable precursor for GY synthesis. However, the HPB exhibits chemical inertness to metathesis due to the proposed steric effect that derives from the metathesis of six propynyl substituted on benzene ring.[29] The steric effect could be decreased through reducing the number of propynyl on benzene ring.

Xiao and coworkers[30] synthesized a graphyne-like porous material through alkyne metathesis reaction using 1,3,5-tripynylbenzene (TPB) as the precursor. They used a commercial available tris(*t*-butoxy)(2,2-dimethylpropylidyne)-tungsten (VI) as the catalyst. The synthesized carbon-rich network presents n-type semiconductor property with a low work function of 3.9 eV and a reduction potential of –0.54 V (vs. SHE) and also exhibits favorable gas adsorption ability.[30] However, the tungsten (VI) complexes are with high price and very sensitive to air, leading to graphyne-like structure preparation with high cost. In 2003, Chauvin and coworkers[31] developed an instant catalyst originally generated in situ from $Mo(CO)_6$-*p*-chlorophenol, which not only exhibits high efficiency toward alkyne metathesis, but also has low cost. In this work, we synthesized a film-like carbon-rich framework which is named as

Dr. J. Q. Li, C. Yin, Prof. L. M. Tong, Prof. J. Zhang
Center for Nanochemistry
Beijing Science and Engineering Center for Nanocarbons
Beijing National Laboratory for Molecular Sciences
College of Chemistry and Molecular Engineering
Peking University
Beijing 100871, P. R. China
E-mail: jinzhang@pku.edu.cn
S. Li, Q. Liu, Prof. C. G. Chen
School of Chemistry and Chemical Engineering
Chongqing University
Chongqing 401331, P. R. China
E-mail: cgchen@cqu.edu.cn
The ORCID identification number(s) for the author(s) of this article can be found under https://doi.org/10.1002/smll.201805344.

DOI: 10.1002/smll.201805344

hydrogen substituted graphyne (HsGY) through alkyne metathesis reaction using TPB as precursor. Considering the extended π-conjugated carbon skeleton comprised of acetylic linkages and benzene ring, we use the synthesized HsGY as a sulfur host matrix to apply in lithium–sulfur batteries (LSBs). The unique structure of HsGY makes it has high Li^+ mobility and short sulfur energy-storing unites. The micropores (≈1 nm) of HsGY could encapsulate the sulfur and essentially confine soluble polysulfide (LiPSs) dissolution, therefore alleviating the "shuttle effect" in LSBs system.

The schematic illustration of synthetic strategy and characterization of HsGY are depicted in **Figure 1**. The detailed synthetic procedures are provided in Figure S1 in the Supporting Information. The ether-stabilized catalyst was first formed in situ in the presence of $Mo(CO)_6$ and 2-fluorophenol in chlorobenzene. During the alkyne metathesis reaction, the 2-butyne (boiling point ≈27 °C) was released as a side product. The concentration in the gas/liquid interface is lower than that in liquid. Therefore, the GY film is readily to form on the gas/liquid interface due to the low concentration of 2-butyne that will drive the equilibrium toward product formation. Figure 1b shows the HsGY film after reaction. The morphology of the as-prepared HsGY film was characterized by scanning electron microscopy (SEM). Figure 1c shows that the film has a smooth and continuous surface. Atomic force microscopy (AFM) characterization of HsGY film further indicates that the film has a smooth surface and the thickness is about 1.1 µm (Figure 1d). Transmission electron microscopy (TEM) image indicates the film-like structure of as-obtained HsGY film (Figure S2a, Supporting Information). High-resolution TEM (HRTEM) characterization clearly reveals the curved streaks with a lattice parameter of 0.352 nm, which could be assigned to the interlayer distance of HsGY (Figure 1e).[30] Energy-dispersive spectroscopy (EDS) elemental mapping characterized results show that the carbon element is located on the whole film (**Figure 2**f–i) consisted of single point analysis of EDS (Figure S2b, Supporting Information) results. The existence of little oxygen might result from the SiO_2/Si plate or inevitable defects.

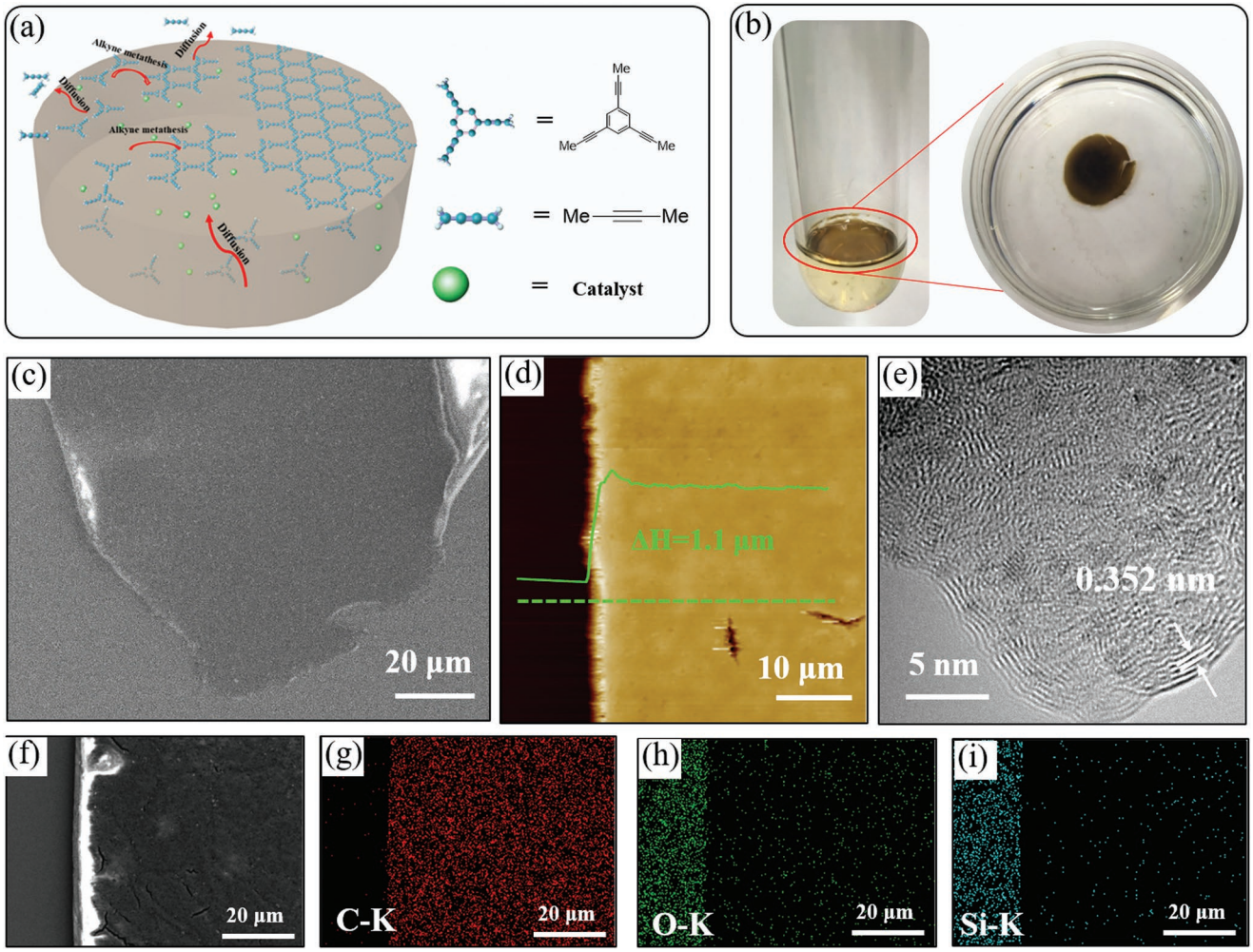

Figure 1. a) Schematic illustration of the experimental setup for the HsGY synthesis through alkyne metathesis reaction. b) Images of HsGY film formed on gas/liquid interface after reaction completed. c) SEM images of HsGY film on SiO_2/Si plate. d) AFM image of HsGY on SiO_2/Si plate. e) HRTEM image and f–i) Elemental mapping of HsGY film.

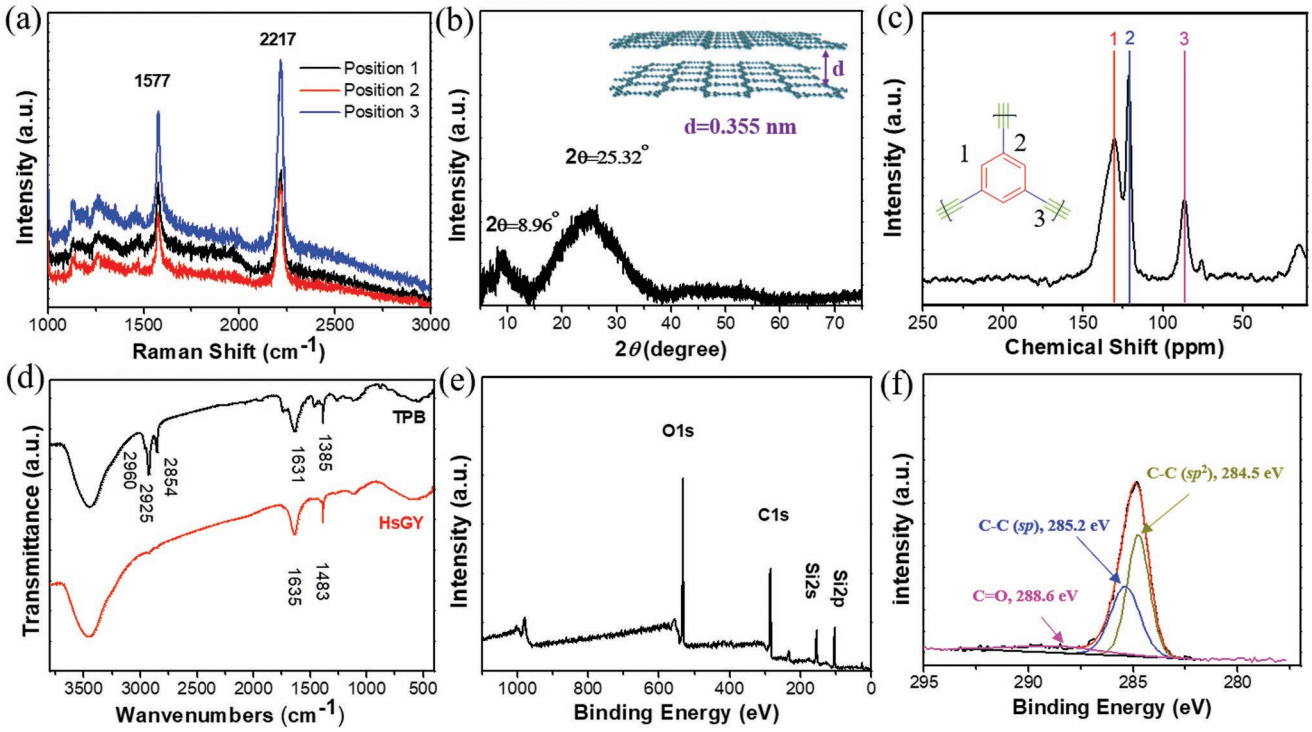

Figure 2. a) Raman spectra of HsGY film on SiO_2/Si plate. b) XRD patterns of HsGY. c) ^{13}C Solid-state ^{13}C NMR spectrum of HsGY. d) FT-IR spectra of HsGY and TPB. e) Survey scan and f) C1s narrow scan XPS of HsGY film on SiO_2/Si plate.

The bonding structure and crystal structure of HsGY were studied systemically by Raman spectroscopy, X-ray diffraction (XRD), solid-state NMR, Fourier transform infrared spectroscopy (FT-IR), and X-ray photoelectron spectroscopy (XPS). Figure 2a shows the typical Raman spectra of HsGY film at different positions. In the Raman spectra of HsGY film, two dominant peaks appear at 1577 and 2217 cm^{-1}, respectively. The peak at 1577 cm^{-1} comes from the vibration of carbon–carbon double bonds in benzene ring and some other peaks appeared at 1129, 1259, and 1462 cm^{-1}. The peak at 2217 cm^{-1} is attributed to the stretching vibration of carbon–carbon triple bonds (−C≡C−).[30] Figure S4 in the Supporting Information displays the typical Raman spectrum of monomer (TPB), in which five dominant peaks appeared at 1346, 1586, 2231, 2264, and 2918 cm^{-1}, respectively. Bathochromic shift is observed in the Raman spectrum of HsGY compared with the spectrum of HPB due to the extensive conjugated π-system formed after alkyne metathesis reaction. Moreover, the carbon–hydrogen bonds in methyl were not detected in HsGY, which means the alkyne metathesis reaction occurred. We note that no obvious changes of the HsGY film were observed during the Raman spectroscopic characterization by 633 nm laser with multiple tests (Figure S5, Supporting Information), indicating the good stability of the synthesized HsGY in air.[22] The XRD result of the as-synthesized sample is shown in Figure 2b. The peak at 25.32° corresponds to the interlayer spacing of 0.355 nm,[30] which is a smaller interlayer distance compared to graphdiyne.[9] The diffraction peak at 8.89° corresponds to the diffraction spacing of 0.995 nm, which is indexed as a set of (110) diffractions derived from a hexagonal 2D lattice with $a = b = 1.194$ nm of HsGY structure (Figure S6, Supporting Information). To further confirm the structure of HsGY, the solid-state NMR experiment was carried out. As shown in Figure 2c, three kinds of carbon mainly exist in the HsGY framework. The peaks at 130.6 and 121.5 ppm correspond to the carbon atom in the benzene ring, which are connected to the hydrogen and sp hybrid carbon atom in ethynyl, respectively.[32] The peaks at 86.5 ppm can be ascribed to sp hybrid carbon atom.[30] Figure 2d displays the FT-IR spectra of TPB and HsGY. In the spectrum of TPB, the bands located at 1381 and 1631 cm^{-1} are assigned to the skeletal vibrations of aromatic ring. The bands from 2654 cm^{-1} to 2960 cm^{-1} are the typical carbon–hydrogen stretching vibration of methyl groups in TPB. In the spectrum of HsGY, the stretching vibration and bending vibration of aromatic ring also can be observed at 1432 and 1587 cm^{-1}. The peaks at 800–1200 cm^{-1} may be attributed to the in-plane and out-plane bending vibration stretching of carbon–hydrogen bonds on benzene ring. XPS measurements indicate that the film is mainly composed of carbon element (Figure 2e). The existence of Si and part of oxygen results from the SiO_2/Si substrate. The peak at 285.0 eV shows essentially identical binding energy for the C1s orbital (Figure 2f), which can be deconvoluted into four subpeaks at 284.5, 285.2, and 288.6 eV, assigned to the C1s orbital of C=C, C≡C, and C=O bonds, respectively. The small amount of oxygen might result from the adsorption of oxygen from air or the inevitable defects, which is in agreement with EDS elemental mapping results (Figure 1f–i).

The designed electrode configuration of LSBs is illustrated in **Figure 3**a, in which HsGY@S was served as a cathode. S_8 was introduced into HsGY conductive matrix, and the residual sulfur was removed by CS_2 washing. Thanks to the mesoporous nature and alkyne-rich structure, the HsGY can not only

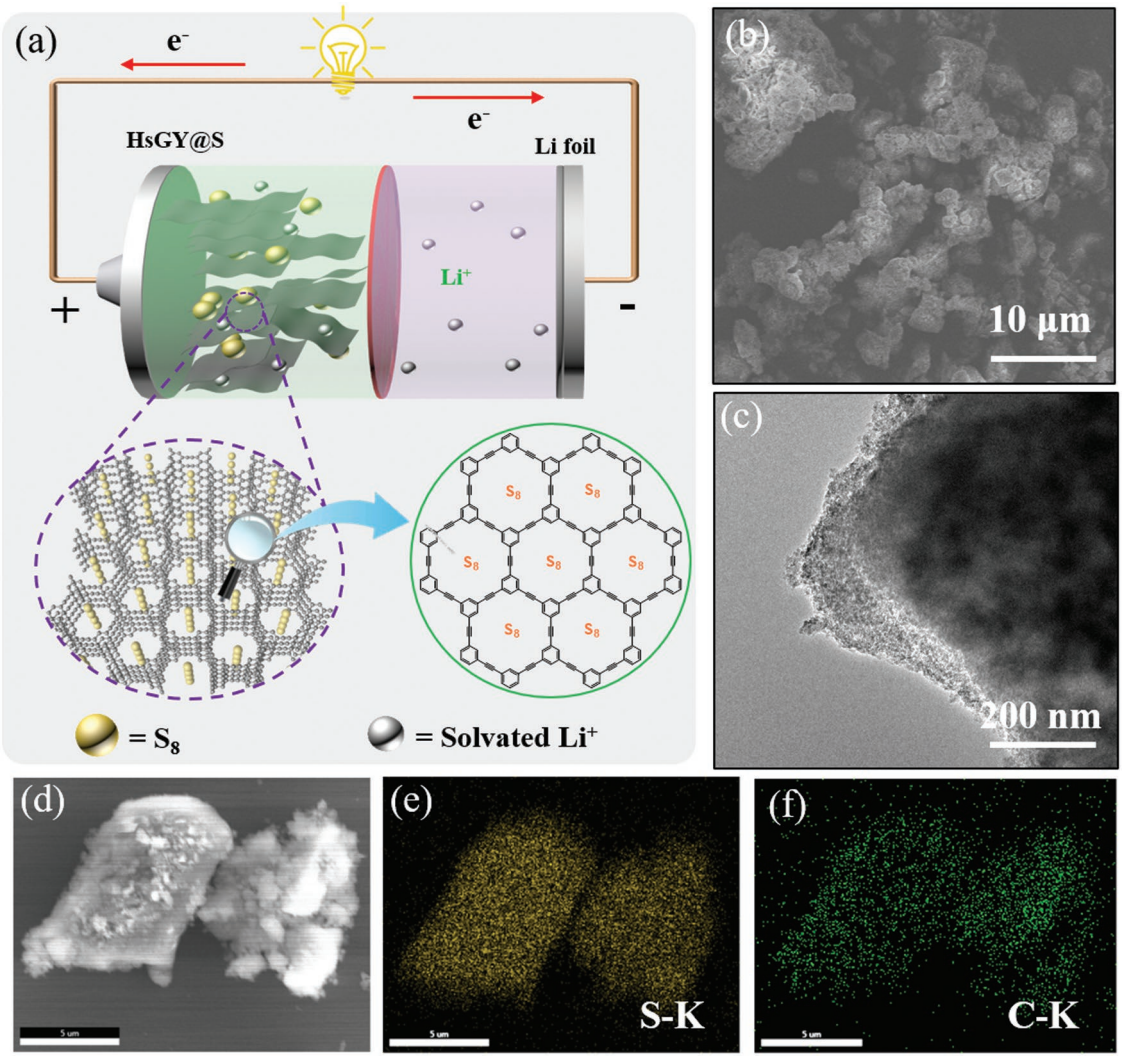

Figure 3. a) Schematic illustration of the electrode configuration for the designed LSB with a HsGY@S electrode. b) SEM image of HsGY@S. c) TEM image of HsGY@S. d–f) EDXelemental mapping of HsGY@S composite.

physically trap soluble LiPSs, but also avail to improve electrical conductivity of sulfur cathode due to the triangular pores of HsGY by chemically bonding to carbon–carbon triple bonds,[33] the as-prepared HsGY@S composite with the accessible surface area, and the broad pathway instead of aggregation, can offer enough internal space to facilitate the soak of electrolyte and accommodate volumetric expansion during cycling. In order to compare with other carbon material, we prepared reduction graphene oxide (rGO)@S composite using the same preparation method. The morphology, nanostructure, and elemental composition of as-synthesized HsGY@S were characterized by SEM, TEM, and EDS. SEM images are depicted in Figure 3b. The morphology of HsGY@S becomes amorphous (Figure 3c), remaining void space in the porous carbon layer that can accommodate large volume changes of sulfur cathode during charge–discharge cycle. Elemental mapping results of HsGY@S composite confirm that sulfur has been successfully introduced into loading matrix, which emerges as a uniform distribution (Figure 3d–f).

Further component characterization of pristine HsGY and HsGY@S were performed by Raman spectroscopy (**Figure 4**a). Both Raman spectra of HsGY and HsGY@S present two prominent peaks at 1576 and 2218 cm^{-1}, respectively. The peak at 1576 cm^{-1} was assigned to the stretching vibration of sp^2 carbon lattice in aromatic ring,[34] and the other one was derived from the vibration of the carbon–carbon triple bonds. Weaker density of carbon–carbon triple bonds was observed in HsGY@S compared to pristine HsGY, indicating part of carbon–carbon triple bonds of HsGY react with sulfur to generate C–S bonds (735 cm^{-1}) and S–S bonds, which are observed in the Raman spectrum of HsGY@S.[35] As is shown in Figure 4b, the exclusive broad peak around 25.32° in the XRD pattern of HsGY is derived from the interlayer spacing of 0.355 nm.[30] After sulfur impregnation, XRD pattern of the as-obtained composite indicates cubic sulfur (JCPDS No. 08-0247) and HsGY.[36] Figure 4c shows the FT-IR spectra of pristine HsGY and HsGY@S. There are nearly no differences between HsGY and HsGY@S except that the prominent band near 647 and 804 cm^{-1} that are

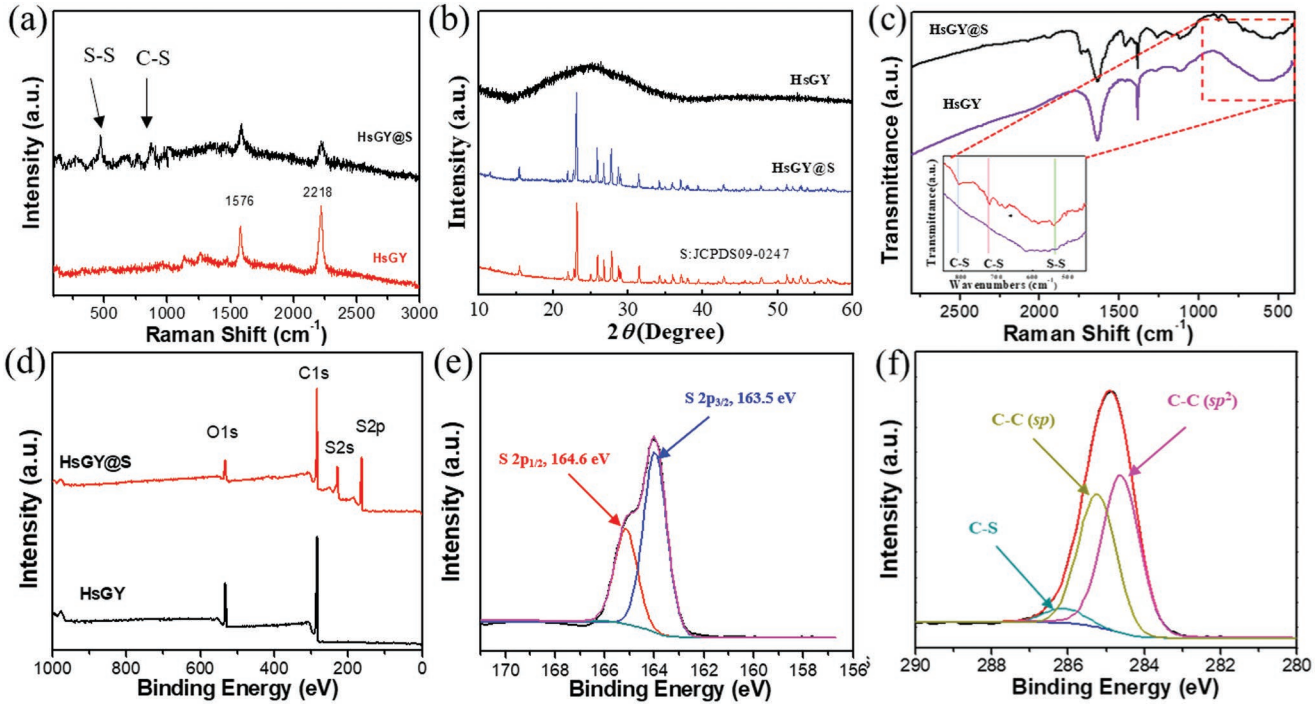

Figure 4. a) Raman spectra, b) XRD patterns, and c) FT-IR spectra of HsGY@S and rGO@S. d) Survey XPS of HsGY@S and HsGY. High-resolution XPS of S2p e) and C1s f) of the HsGY@S.

assigned to C–S bonds. And the band appeared at 519 cm^{-1} is responding to S–S bonds, which is consistent with the Raman result (Figure 4c inset).[37] As displayed in XPS of HsGY@S in Figure 4d, sulfur element is obvious indicating the successful impregnation of sulfur. The narrow spectra of S2p can be resolved into two peaks located at around 163.5 eV ($S2p_{3/2}$) and 164.6 eV ($S2p_{1/2}$), having an energy separation of 1.1 eV, confirming the presence of C–S bonds instead of elemental sulfur whose $S2p_{3/2}$ peak located at 164.0 eV (Figure 4e).[38,39] As shown in Figure 4f, two fitted peaks with binding energies at ≈284.6 and 285.2 eV are discovered in the high-resolution C1s XPS, revealing the existence of C–C double and C–C triple bonds,[40] respectively. Furthermore, C1s XPS of HsGY@S has an additional peak at 286.1 eV, assigned to C–S bonds.[41] Thermogravimetric analysis (TGA) was applied to obtain the thermal behavior of HsGY, HsGY@S, and rGO/S. As displayed in Figure S7 in the Supporting Information, the amount of sulfur in HsGY@S and rGO/S composites is 74.7 wt% and 67.2 wt%. Interestingly, HsGY@S maintains superior sulfur loading by its triangular pores and has a higher mass reduction temperature, revealing that it endows a better encapsulated sulfur property, and exerts a better thermal stability. Regarding the weight loss of HsGY, there are two main mass losses. The first one at around room temperature to 240 °C can be related to the loss of free water and bonded water and the second loss (at around 380–600 °C) can probably be ascribed to oligomeric volatiliation derived from TPB precursor.

The electrochemical performance of HsGY@S was examined in CR2032 coin cells where Li metal served as the negative electrode. Before evaluating the electrochemical performance, visualized adsorption tests were conducted and demonstrated the strong adsorption ability of Li_2S_6 by HsGY (Figure S8, Supporting Information). Additionally, ultraviolet–visible (UV–vis) absorption measurement of HsGY@S presents that strong absorbance peak in HsGY in the visible light area was not easily to be detected,[42] revealing its strong adsorbability of polysulfide ions. It can be speculated that this strong adsorbability property of HsGY is derived from the extended π-conjugated carbon skeleton comprised of acetylic linkages and benzene rings. Furthermore, the rich micropores (≈1 nm) on the surface of HsGY is beneficial to encapsulate polysufide species and thus avoid their dissolution. **Figure 5**a presents the initial cyclic voltammogram (CV) profiles of HsGY@S and rGO@S electrodes in a voltage window of 1.7 to 2.8 V (vs Li/Li^+) at a scan rate of 0.1 mV s^{-1}. Both HsGY@S and rGO@S present two cathodic peaks that correspond to the ring-opening reduction of sulfur (S_8) to form soluble high-order lithium polysulfides (LiPSs), for example, Li_2Sx ($4 \le x \le 8$), and then insoluble low-order LiPSs (Li_2S_2/Li_2S). As to the reverse anodic scan, rGO@S electrode manifests one anodic peak at around 2.42 V (vs Li/Li^+), attributed to the conversion of Li_2S_2/Li_2S to S_8.[43] By contrast, HsGY@S electrode displays two apparent anodic peaks between 2.3 and 2.4 V (vs Li/Li^+), speculating that LiPSs are efficiently entrapped and oxidated adequately to S_8 in the alkyne-rich system and unique triangular pores of HsGY host by chemically bonding to carbon–carbon triple bonds during the charge process.[44] Compared to the rGO@S electrode, the sharper peaks and smaller potential gaps can be observed in CV profile of HsGY@S (Figure S9a, Supporting Information), which reveals HsGY@S electrode with enhanced electrochemical kinetic process and decreased electrochemical polarization in LSBs system.[45] Moreover, the onset potential of the HsGY@S electrode in the

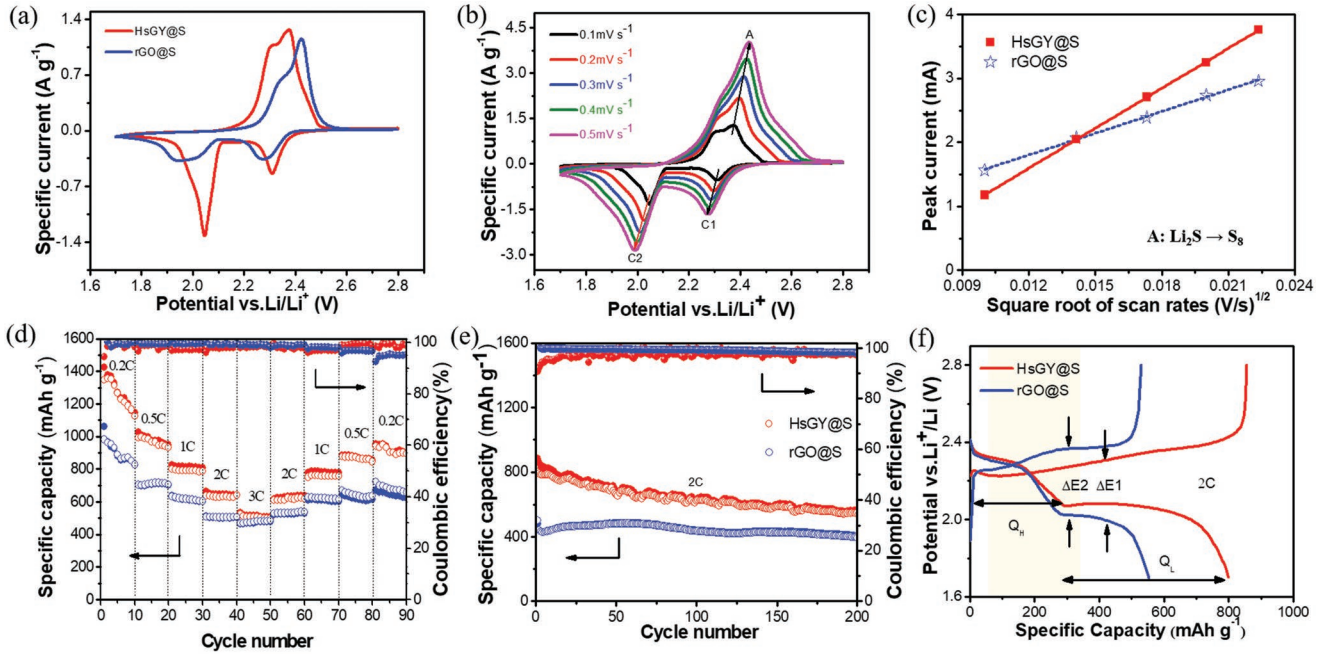

Figure 5. a) CV curves (0.1 mV s^{-1}) of the HsGY@S and rGO@S electrodes. b) CV profiles of HsGY@S electrodes at various scan rates. c) Plots of anodic peak current of the HsGY@S and rGO@S electrodes as a function of their corresponding the square root of scan rates. d) Rate capacities of the HsGY@S and rGO@S electrodes. e) Long-term cycling and Coulombic efficiency of the HsGY@S and rGO@S electrodes at 2 C. f) Galvanostatic charge/discharge profiles of the HsGY@S and rGO@S electrodes at 2 C in the first cycle.

reduction process are higher than pristine rGO@S electrode, while the onset potential is much lower during the oxidation process (Figure S9b,c, Supporting Information), demonstrating that HsGY@S electrode has prominent reaction kinetics.[46] Figure 5b displays the CV profiles of HsGY@S at various scan rate from 0.1 to 0.5 mV s^{-1}. All the cathodic and anodic I_P show linear relationships with the square root of scanning rates (Figure 5c, Figure S9d,e, Supporting Information), demonstrating a typical diffusion-controlled reaction.[47,48] The calculating results of D_{Li}^+ (Li^+ diffusion coefficient) are summarized in Table S1 in the Supporting Information. Compared with the rGO@S electrode, the HsGY@S electrode presents the higher D_{Li}^+, which is also manifested in our previous work on lithium-ion batteries (LIBs) electrochemical mechanism.[49] The rate capability of the HsGY@S and rGO@S electrode was tested at different current densities (Figure 5d). As the current density increasing from 0.2 to 1 C, HsGY@S electrode displays reversible and stable capacities from 1312 to 799 mAh g^{-1}, respectively. A stable capacity of 507 mAh g^{-1} remains even at a high current density of 3 C. When the current rate gradually returned to 2, 1, 0.5, and 0.2 C, the discharge capacities reverted to 614, 779, 885, and 954 mAh g^{-1}. The rGO@S electrode delivered reversible capacities of 981, 703, 632, 509, and 470 mAh g^{-1} from 0.2 to 3 C, respectively, which are lower than HsGY@S at same current density. Figure S9f in the Supporting Information depicts the corresponding first cycle galvanostatic charge/discharge curves of HsGY@S electrode at varying rates with the voltage range from 1.7 to 2.8 V (vs Li/Li^+). The dual discharging platforms and a single charge platform of above curves could be seen clearly, which corresponds to the aforementioned CV results. Despite a high rate of 3 C, the two discharge plateaus and a single charge plateau of the HsGY@S electrode profiles are still maintained, resulting from the conductive carbon skeleton with triangle-like pores structure and high Li^+ mobility. Figure 5e presents the long-term cycling performance of the as-synthesized HsGY@S and rGO@S electrodes at a current rate of 2 C. Compared with rGO@S, the HsGY@S electrode presents a good cycling stability, exhibiting an initial reversible capacity of 881 $mAhg^{-1}$ and finally stabilizing at 557 mAh g^{-1} after 200 cycles, much larger than that of rGO@S (479 mA h g^{-1}) even obtained at the first cycle. This superior cycling durability of HsGY@S can be speculated due to: 1) the highly dispersed active sulfur particles in the channels of HsGY host reducing the mass transport of redox species. 2) the strong adsorbability property of HsGY to LiPSs alleviating the "shuttle" effect. 3) the high electronic conductivity and large Li^+ transit property facilitating the reaction kinetics.[50] Additionally, a comparison of potential difference (represented by ΔE) for HsGY@S and rGO@S electrodes between the initial charge/discharge potential platforms at 2 C rate is displayed in Figure 5f, where the ΔE_1 and ΔE_2 are 0.20 and 0.34 V, respectively. Generally speaking, the value of ΔE is relevant to electrochemical polarization in the cycling charge/charging process.[50] Therefore, HsGY@S electrode possesses smaller polarization and faster reaction kinetics. Ideally, the discharge capacity of the second plateau (Q_L) is three times higher than the discharge capacity of the first plateau (Q_H). In fact, the solid-state diffusion and the higher order LiPSs diffusion in the second plateau leads to the value of $Q_L/Q_H < 3$.[51] As to HsGY@S electrode, the value of Q_L/Q_H is higher than that of the rGO@S electrode. Based on the above analysis, it can be further confirmed the HsGY can effectively optimize the reduction of LiPSs to insoluble Li_2S species.

The electrochemical impedance spectroscopy (EIS) measurements were performed to determine the kinetics mechanism of enhanced electrochemical performance of as-prepared HsGY@S. As shown in Figure S9h in the Supporting Information, the Nyquist plot of the HsGY@S electrode displays a high frequency semicircle and an oblique low-frequency line, corresponding to the charge-transfer resistance (R_{ct}) and the Li^+ diffusion resistance (W_e) in the electrode, respectively. Moreover, the high-frequency semicircle intercepted on the *X*-axis is related to the electrolyte resistance (R_e).[52] The relevant resistance fitting values of two electrodes are listed in the Table S2 in the Supporting Information. It is visibly seen that the R_{ct} value of HsGY@S electrode after 10th cycles is ≈31.37 Ω and after 200th cycles is≈15.48 Ω, respectively, which are much lower than fresh electrodes (≈34.92 Ω), resulting from homogeneous redistribution of active sulfur within the alkyne-rich system and unique triangular pores of HsGY after cycling. And concentration gradient force is formed between electrolyte and solid-state electrode by the transmission of polysulfide ions, which favors optimized electrochemical reactions, improved ions kinetic diffusion, and ameliorative infiltration capacity to reduce the electrochemical polarization. With respect to the impedance spectra of the cycled rGO@S electrode, as shown in Figure S9i in the Supporting Information, two depressed high-to-medium frequency semicircles with a long sloping line were observed in the low frequency region. The first semicircle in high-frequency region is associated with R_{ct} as well, while the medium-frequency semicircle may be related to an accumulated insulating layer on the surface of Li anode by insoluble discharging Li_2S_2 or Li_2S species.[53] Notably, the HsGY@S electrode presents only one semicircle in high-to-medium frequency region, indicating fast Li^+ mobility into the sulfur electrode and prevention of the LiPSs reduction in the lithium anode. Overall, the HsGY@S electrode demonstrates the superior electrochemical performance for LSBs application confirmed by the above EIS results and all preceding measurements.

In summary, we synthesized HsGY film in the gas/liquid interface through alkyne metathesis reaction using TPB as the precursor. The synthesized HsGY film presents a layer-like structure and can be used as a sulfur host matrix for LSBs application due to its extended π-conjugated carbon skeleton comprised of acetylic linkages and benzene rings. Electrochemical test results indicate that HsGY@S electrode exhibits high reversible capacity and stable long term cycling performance, which make HsGY could be used as a promising sulfur host material applied in practical LSBs after further study in the future.

Experimental Section

Hydrogen Substituted Graphyne (HsGY) Preparation: Under Ar atmosphere, to a 25 mL Schlenk flask was added 10 mg TPB, 2 mg $Mo(CO)_6$, 2 mL anhydrous chlorobenzene, and 50 µL 2-fluorophenol continuously. Then the reaction mixture was heated to 135 °C for 8 to 24 h without stirring. In order to form large flakes, the efficient removal of 2-butyne was necessary. The reaction mixture was then exposed to a vacuum for five times at 30 min intervals across 2.5 period. After the reaction completed, a carbon film formed on the interface of solvent. The film was washed by acetone, toluene, and water continuously to obtain HsGY.

Synthesis of HsGY@S Composite: Melt-diffusion strategy was adopted to prepare the HsGY@S composite. Precisely, the as-prepared HsGY and sublimed sulfur (1:9, weight ratio) were well mixed by hand-milled for 30 min to yield a black mixture. Afterward, the mixture was heated at 155 °C for 12 h in 50 mL Teflon-lined autoclave. More importantly, the product was dissolved in CS_2 for 30 s to remove the excrescent sulfur outside of the HsGY and then dried at 50 °C under vacuum, tagged as HsGY@S composite. Comparatively, sulfur was implanted into the reduction graphene oxide (rGO) with the routine mentioned above. The encapsulated sulfur composite was collected as rGO@S.

Supporting Information

Supporting Information is available from the Wiley Online Library or from the author.

Acknowledgements

J.Q.L. and S.L. have contributed equally to this work. This work was supported by the Ministry of Science and Technology of China (2016YFA0200101 and 2016YFA0200104) and the National Natural Science Foundation of China (Grant Nos. 51432002, 51720105003, and 21790052)

Conflict of Interest

The authors declare no conflict of interest.

Keywords

alkyne metathesis reaction, dynamic reaction, hydrogen substituted graphyne, lithium–sulfur batteries

Received: December 15, 2018
Revised: January 19, 2019
Published online: March 1, 2019

[1] L. Dai, Y. Xue, L. Qu, H. J. Choi, J. B. Baek, *Chem. Rev.* **2015**, *115*, 4823.
[2] H. W. Kroto, J. R. Heath, S. C. Obrien, R. F. Curl, R. E. Smalley, *Nature* **1985**, *318*, 162.
[3] S. Iijima, *Nature* **1991**, *354*, 56.
[4] K. S. Novoselov, A. K. Geim, S. V. Morozov, D. Jiang, Y. Zhang, S. V. Dubonos, I. V. Grigorieva, A. A. Firsov, *Science* **2004**, *306*, 666.
[5] X. Zhang, D. Liu, L. Yang, L. Zhou, T. You, *J. Mater. Chem. A* **2015**, *3*, 10031.
[6] L. Zhao, X.-L. Sui, J.-L. Li, J.-J. Zhang, L.-M. Zhang, Z.-B. Wang, *Catal. Commun.* **2016**, *86*, 46.
[7] H. Song, Q. Zhu, X.-j. Zheng, X. Chen, *J. Mater. Chem. A* **2015**, *3*, 10368.
[8] F. Yavari, Z. Chen, A. V. Thomas, W. Ren, H. M. Cheng, N. Koratkar, *Sci. Rep.* **2011**, *1*, 166.
[9] J. Li, J. Xu, Z. Xie, X. Gao, J. Zhou, Y. Xiong, C. Chen, J. Zhang, Z. Liu, *Adv. Mater.* **2018**, *30*, 1800548.
[10] B. Luo, L. Zhi, *Energy Environ. Sci.* **2015**, *8*, 456.
[11] J. He, N. Wang, Z. Cui, H. Du, L. Fu, C. Huang, Z. Yang, X. Shen, Y. Yi, Z. Tu, Y. Li, *Nat. Commun.* **2017**, *8*, 1172.
[12] A. L. Ivanovskii, *Prog. Solid State Chem.* **2013**, *41*, 1.
[13] A. R. Puigdollers, G. Alonso, P. Gamallo, *Carbon* **2016**, *96*, 879.

[14] R. H. Baughman, H. Eckhardt, M. Kertesz, *J. Chem. Phys.* **1987**, *87*, 6687.
[15] J. Zhou, Z. Xie, R. Liu, X. Gao, J. Li, Y. Xiong, L. Tong, J. Zhang, Z. Liu, *ACS Appl. Mater. Interfaces* **2018**, *11*, 2632.
[16] B. Kang, J. Y. Lee, *J. Phys. Chem. C* **2014**, *118*, 12035.
[17] Y. Li, L. Xu, H. Liu, Y. Li, *Chem. Soc. Rev.* **2014**, *43*, 2572.
[18] D. W. Ma, T. Li, Q. Wang, G. Yang, C. He, B. Ma, Z. Lu, *Carbon* **2015**, *95*, 756.
[19] M. M. Haley, S. C. Brand, J. J. Pak, *Angew. Chem., Int. Ed. Engl.* **1997**, *36*, 836.
[20] G. Li, Y. Li, H. Liu, Y. Guo, Y. Li, D. Zhu, *Chem. Commun.* **2010**, *46*, 3256.
[21] J. Zhou, X. Gao, R. Liu, Z. Xie, J. Yang, S. Zhang, G. Zhang, H. Liu, Y. Li, J. Zhang, Z. Liu, *J. Am. Chem. Soc.* **2015**, *137*, 7596.
[22] J. Li, Z. Xie, Y. Xiong, Z. Li, Q. Huang, S. Zhang, J. Zhou, R. Liu, X. Gao, C. Chen, L. Tong, J. Zhang, Z. Liu, *Adv. Mater.* **2017**, *29*, 1700421.
[23] R. Matsuoka, R. Sakamoto, K. Hoshiko, S. Sasaki, H. Masunaga, K. Nagashio, H. Nishihara, *J. Am. Chem. Soc.* **2017**, *139*, 3145.
[24] H. Yang, Y. Jin, Y. Du, W. Zhang, *J. Mater. Chem. A* **2014**, *2*, 5986.
[25] F. E. Goodson, T. I. Wallow, B. M. Novak, *J. Am. Chem. Soc.* **1997**, *119*, 12441.
[26] A. Mortreux, O. Coutelier, *J. Mol. Catal. A: Chem.* **2006**, *254*, 96.
[27] B. Haberlag, M. Freytag, C. G. Daniliuc, P. G. Jones, M. Tamm, *Angew. Chem., Int. Ed.* **2012**, *51*, 13019.
[28] V. Maraval, C. Lepetit, A.-M. Caminade, J.-P. Majoral, R. Chauvin, *Tetrahedron Lett.* **2006**, *47*, 2155.
[29] O. Š. Miljanić, K. P. C. Vollhardt, G. D. Whitener, *Synlett* **2003**, *1*, 29.
[30] B. Wu, M. Li, S. Xiao, Y. Qu, X. Qiu, T. Liu, F. Tian, H. Li, S. Xiao, *Nanoscale* **2017**, *9*, 11939.
[31] V. Huc, R. Weihofen, I. Martin-Jimenez, P. Oulié, C. Lepetit, G. Lavigne, R. Chauvin, *New J. Chem.* **2003**, *27*, 1412.
[32] N. Wang, J. He, Z. Tu, Z. Yang, F. Zhao, X. Li, C. Huang, K. Wang, T. Jiu, Y. Yi, Y. Li, *Angew. Chem., Int. Ed.* **2017**, *56*, 10740.
[33] P. T. Dirlam, A. G. Simmonds, T. S. Kleine, N. A. Nguyen, L. E. Anderson, A. O. Klever, A. Florian, P. J. Costanzo, P. Theato, M. E. Mackay, R. S. Glass, K. Char, J. Pyun, *RSC Adv.* **2015**, *5*, 24718.
[34] S. Zhang, J. Wang, Z. Li, R. Zhao, L. Tong, Z. Liu, J. Zhang, Z. Liu, *J. Phys. Chem. C* **2016**, *120*, 10605.
[35] J. S. Kim, T. H. Hwang, B. G. Kim, J. Min, J. W. Choi, *Adv. Funct. Mater.* **2014**, *24*, 5359.
[36] M. Chen, S. Jiang, C. Huang, J. Xia, X. Wang, K. Xiang, P. Zeng, Y. Zhang, S. Jamil, *ACS Appl. Mater. Interfaces* **2018**, *10*, 13562.
[37] B. Duan, W. Wang, A. Wang, K. Yuan, Z. Yu, H. Zhao, J. Qiu, Y. Yang, *J. Mater. Chem. A* **2013**, *1*, 13261.
[38] Z. Wang, Y. Dong, H. Li, Z. Zhao, H. B. Wu, C. Hao, S. Liu, J. Qiu, X. W. Lou, *Nat. Commun.* **2014**, *5*, 5002.
[39] Q. Pang, J. Tang, H. Huang, X. Liang, C. Hart, K. C. Tam, L. F. Nazar, *Adv. Mater.* **2015**, *27*, 6021.
[40] Q. Xiang, Y. Liu, X. Zou, B. Hu, Y. Qiang, D. Yu, W. Yin, C. Chen, *ACS Appl. Mater. Interfaces* **2018**, *10*, 10842.
[41] G. Li, J. Sun, W. Hou, S. Jiang, Y. Huang, J. Geng, *Nat. Commun.* **2016**, *7*, 10601.
[42] P. Wang, Z. Zhang, X. Yan, M. Xu, Y. Chen, J. Li, L. Jie, K. Zhang, Y. Lai, *J. Mater. Chem. A* **2018**, *6*, 14178.
[43] L. Wang, Z. Yang, H. Nie, C. Gu, W. Hua, X. Xu, X. Chen, Y. Chen, S. Huang, *J. Mater. Chem. A* **2016**, *4*, 15343.
[44] H. Du, Z. Zhang, J. He, Z. Cui, J. Chai, J. Ma, Z. Yang, C. Huang, G. Cui, *Small* **2017**, *13*, 1702277.
[45] W. Ren, W. Ma, M. M. Umair, S. Zhang, B. Tang, *ChemSusChem* **2018**, *11*, 2695.
[46] C. Zheng, S. Niu, W. Lv, G. Zhou, J. Li, S. Fan, Y. Deng, Z. Pan, B. Li, F. Kang, Q. Yang, *Nano Energy* **2017**, *33*, 306.
[47] X. Tao, J. Wang, C. Liu, H. Wang, H. Yao, G. Zheng, Z. W. Seh, Q. Cai, W. Li, G. Zhou, C. Zu, Y. Cui, *Nat. Commun.* **2016**, *7*, 11203.
[48] Z. Cui, C. Zu, W. Zhou, A. Manthiram, J. B. Goodenough, *Adv. Mater.* **2016**, *28*, 6926.
[49] S. Li, Y. Cen, Q. Xiang, M. K. Aslam, B. Hu, W. Li, Y. Tang, Q. Y. Yu, Y. P. Liu, C. G. Chen, *J. Mater. Chem. A* **2018**, *7*, 1658.
[50] H. Zhang, M. Zhao, X. He, Z. Wang, X. Zhang, X. Liu, *J. Phys. Chem. C* **2011**, *115*, 8845.
[51] D. Gueon, J. T. Hwang, S. B. Yang, E. Cho, K. Sohn, D. K. Yang, J. H. Moon, *ACS Nano* **2018**, *12*, 226.
[52] Z. Liu, S. Bai, B. Liu, P. Guo, M. Lv, D. Liu, D. He, *J. Mater. Chem. A* **2017**, *5*, 13168.
[53] Y. Zhang, K. Sun, Z. Liang, Y. Wang, L. Ling, *Appl. Surf. Sci.* **2018**, *427*, 823.